GDCh Research Article Angewandte International Edition Chemie www.angewandte.org

Check for updates

How to cite: *Angew. Chem. Int. Ed.* **2025**, *64*, e15137
doi.org/10.1002/anie.202515137

Photoenzymes Hot Paper

Miniature Photoenzyme Enables Organelle-Specific Cellular Control via Deboronative Hydroxylation

*Qiaoling Che[+], Ru He[+], Yixin Zhang[+], Haipeng Zhang, Kaixing Zeng, and Yiyun Chen**

Abstract: Artificial photoenzymes hold transformative potential for in vitro biocatalysis, but their translation to live-cell environments demands minimal cellular perturbation and aerobic compatibility. Here, we present miniSOG, a 12 kDa miniature photoenzyme that enables bioorthogonal deboronative hydroxylation via superoxide radical anion ($O_2^{\bullet-}$) generation under blue light irradiation. Leveraging the inherent photochemistry of flavins, miniSOG facilitates the photoactivation of 27 structurally diverse organoboronates—including aryl/alkyl boronates, fluorophores, anticancer agents, and epigenetic modulators—through a unified $O_2^{\bullet-}$-mediated mechanism. This system achieves spatiotemporally precise photocatalysis in live cells, where miniSOG's compact size and subcellular targeting enable organelle-specific localization and confined reactivity due to short-range $O_2^{\bullet-}$ diffusion (~0.2 μm). We demonstrate its utility in light-gated cellular modulation: i) mitochondrial depolarization via localized release of 2,4-dinitrophenol (DNP) to disrupt energy metabolism, and ii) nuclear m^6A methylation enhancement to epigenetically upregulate autophagy. By repurposing miniSOG's photochemistry for bioorthogonal deboronative hydroxylation, this work establishes a versatile, genetically encoded platform for manipulating fundamental cellular pathways with minimal off-target effects.

Introduction

The pursuit of sustainable chemical synthesis has driven innovations in artificial enzymes, particularly photoenzymes, which combine biocatalysis with photocatalysis to harness solar energy for bond formation and cleavage.[1,2] While engineered photoenzymes[3,4] leveraging light-sensitive cofactors like flavins have achieved remarkable success in in vitro asymmetric synthesis (Figure 1a),[5,6] their transition to live-cell environments requires distinct design principles, such as minimal cellular perturbation, genetic encodability, and operation under physiological (aerobic) conditions.[7–10] A key challenge is to develop compact, versatile photoenzymes that can perform bioorthogonal catalysis without perturbing cellular functions.

Optogenetic tools, which rely on light-induced protein conformational changes,[11,12] offer spatiotemporal control but often lack versatility for modulating diverse cellular processes with small-molecule effectors.[13–16] Photoenzymatic systems could bridge this gap by enabling light-triggered generation of bioactive molecules. However, current systems face limitations in substrate tolerance and biocompatibility, hindering bioorthogonal applications. Rather than expanding substrate scope via active-site engineering, we envisioned an alternative strategy that leverages the intrinsic ROS-generating capability of photoenzymes for broad-scope catalysis.

Organoboronic acids have emerged as ideal substrates for bioorthogonal applications due to their biocompatibility, clinical relevance, and chemoselective reactivity.[17,18] Previous works have demonstrated that organic dyes and flavins can photocatalytically generate superoxide radical anion ($O_2^{\bullet-}$) to facilitate deboronative hydroxylation in live cells.[19] While subcellular targeting via genetic encoding is desirable, current hybrid approaches—such as chemical conjugation of dyes to protein scaffolds like SNAP-tag[20–22]—rely on exogenous components and washing steps, introducing practical barriers like background noise, cellular perturbation, and operational complexity in intact systems (Figure 1b).[23,24]

Here, we address these limitations by repurposing miniSOG[25]—a 12 kDa genetically encodable flavoprotein—as a miniature photoenzyme for bioorthogonal catalysis in live cells (Figure 1c). Building on well-established flavin photochemistry,[26–29] miniSOG operates via an oxygen-compatible mechanism: it photocatalytically reduces O_2 to $O_2^{\bullet-}$,[30,31] which then diffuses and mediates deboronative hydroxylation of organoboronates.[32–34] This approach introduces key innovations: The compact size of miniSOG enables

[*] Q. Che[+], R. He[+], Dr. Y. Zhang[+], H. Zhang, K. Zeng, Prof. Y. Chen
State Key Laboratory of Chemical Biology, Shanghai Institute of Organic Chemistry, University of Chinese Academy of Sciences, Chinese Academy of Sciences, 345 Lingling Road, Shanghai 200032, China
E-mail: yiyunchen@sioc.ac.cn

Q. Che[+], R. He[+], K. Zeng, Prof. Y. Chen
School of Physical Science and Technology, ShanghaiTech University, 100 Haike Road, Shanghai 201210, China

Prof. Y. Chen
School of Chemistry and Material Sciences, Hangzhou Institute for Advanced Study, University of Chinese Academy of Sciences, 1 Sub-Lane Xiangshan, Hangzhou 310024, China

[+] These authors contributed equally to this work.

Additional supporting information can be found online in the Supporting Information section

© 2025 Wiley-VCH GmbH

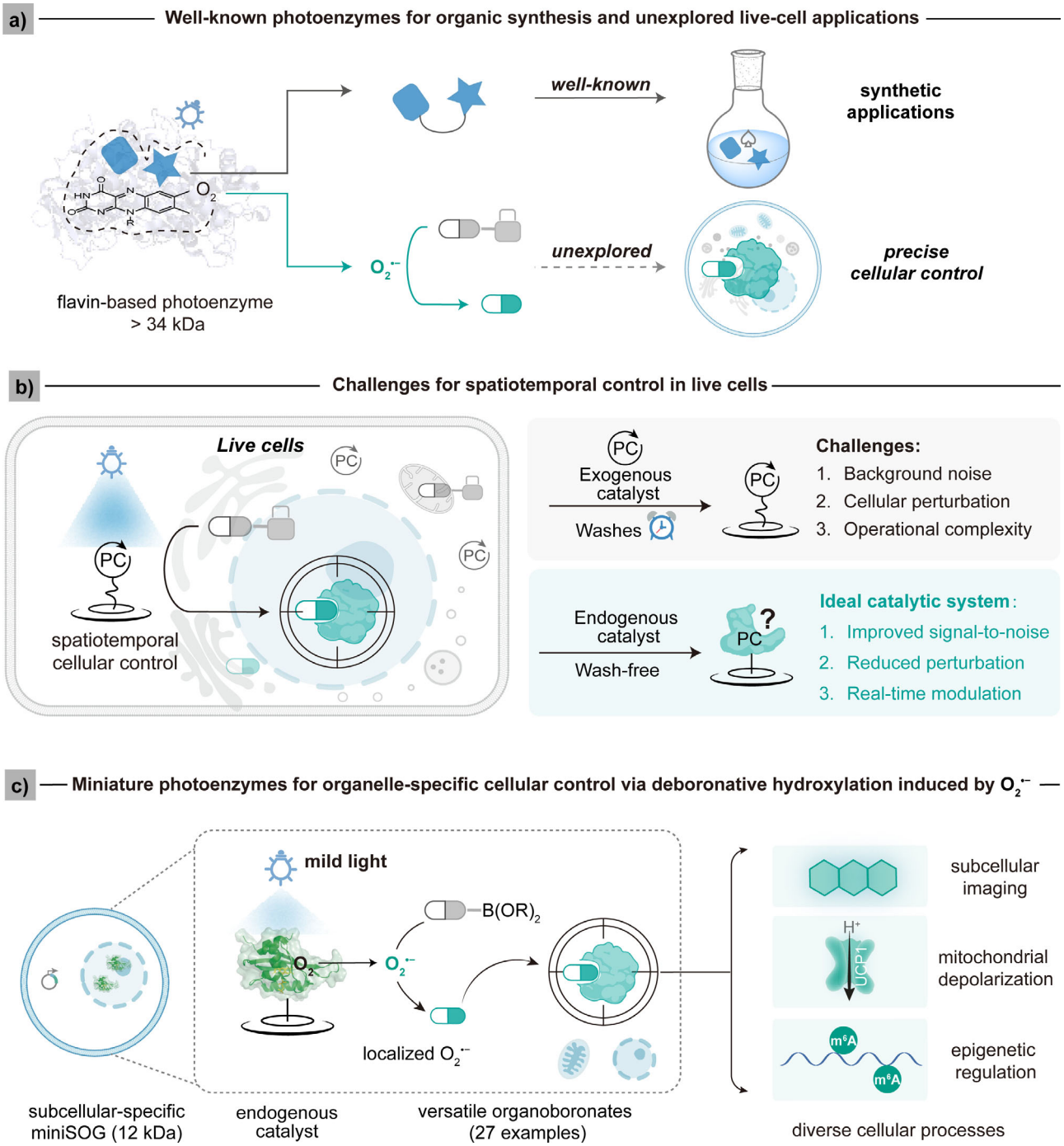

Figure 1. Miniature photoenzymes enable bioorthogonal photocatalysis for organelle-specific cellular control. a) Well-known photoenzymes for organic synthesis and unexplored live-cell applications. b) Challenges for spatiotemporal control in live cells. c) Miniature photoenzymes for organelle-specific cellular control via deboronative hydroxylation induced by $O_2^{\bullet-}$.

precise organelle targeting,[35–38] while short-range $O_2^{\bullet-}$ diffusion (~0.2 μm radius)[21] ensures spatially confined reactivity for broad-scope bioorthogonal reactions. We demonstrate that miniSOG facilitates the activation of 27 structurally diverse organoboronates—including aryl/alkyl derivatives, fluorophores, anticancer agents, and epigenetic modulators—under ambient aerobic conditions, enabling spatiotemporally controlled modulation of cellular processes such as mitochondrial depolarization and epigenetic regulation.

Results and Discussion

Screening of Photoenzymes for Deboronative Hydroxylation

To develop a photoenzyme-based system for bioorthogonal deboronative hydroxylation in live cells, we screened candidates based on key criteria: genetic encodability, compact size for subcellular targeting, and operation under physiological (aerobic) conditions. We evaluated several classes of

© 2025 Wiley-VCH GmbH

15213773, 2025, 51, Downloaded from https://onlinelibrary.wiley.com/doi/10.1002/anie.202515137 by Shanghai Institute Of Organic Chemistry, Wiley Online Library on [16/12/2025]. See the Terms and Conditions (https://onlinelibrary.wiley.com/terms-and-conditions) on Wiley Online Library for rules of use; OA articles are governed by the applicable Creative Commons License

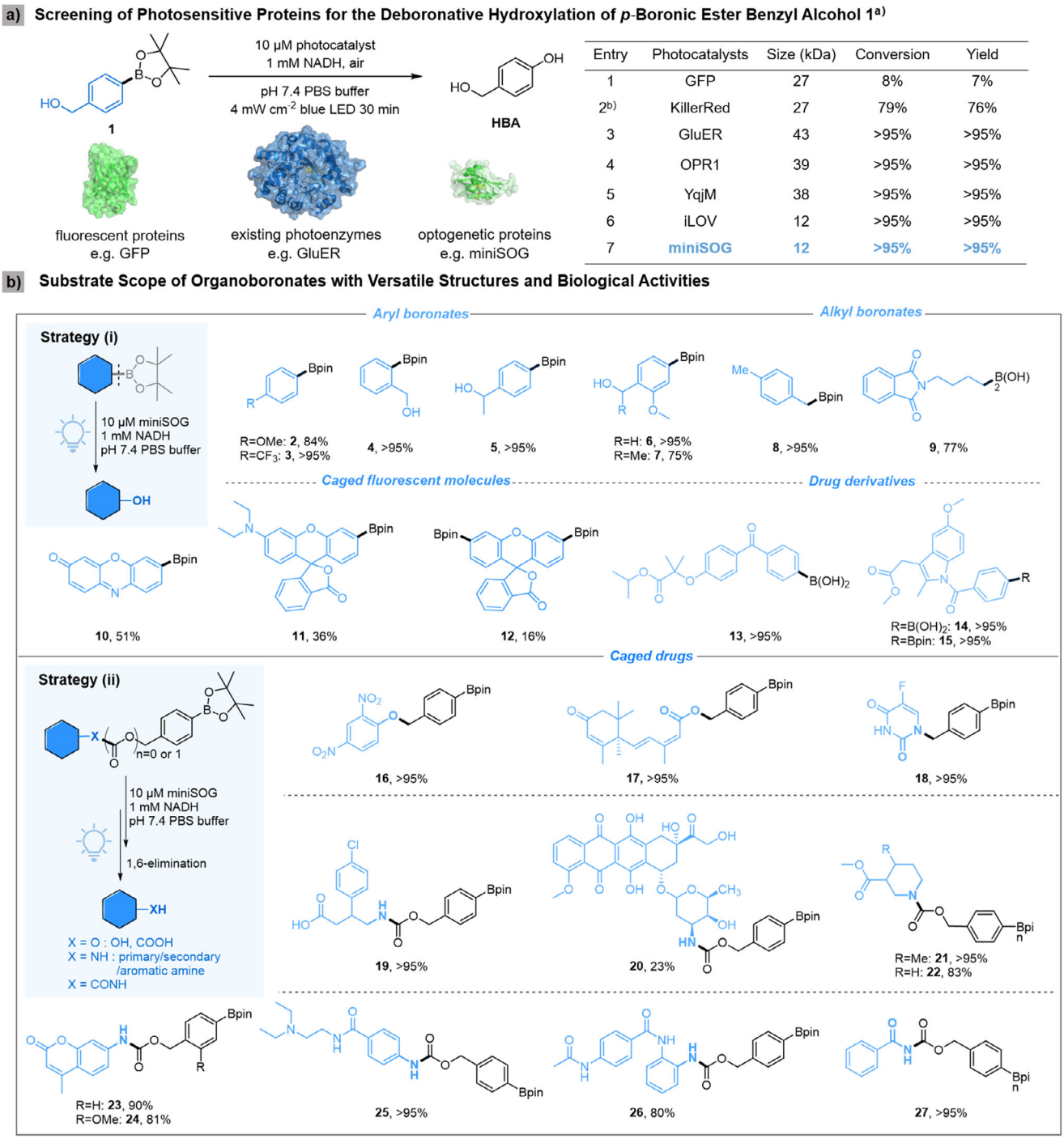

Entry	Photocatalysts	Size (kDa)	Conversion	Yield
1	GFP	27	8%	7%
2[b)]	KillerRed	27	79%	76%
3	GluER	43	>95%	>95%
4	OPR1	39	>95%	>95%
5	YqjM	38	>95%	>95%
6	iLOV	12	>95%	>95%
7	**miniSOG**	**12**	**>95%**	**>95%**

Figure 2. Screening of photoenzymes for deboronative hydroxylation and substrate scope by miniSOG. a) Screening of photosensitive proteins for the deboronative hydroxylation of p-boronic ester benzyl alcohol **1**. b) Substrate scope of organoboronates with versatile structures and biological activities. [a)] Standard reaction conditions: 200 μM **1** or organoboronates, 10 μM photocatalysts, 1 mM NADH, pH 7.4 PBS buffer, 4 mW cm^{-2} blue LED for 30 min. Conversions and yields were determined by HPLC analysis. [b)] Reaction conditions: 20 μM KillerRed, 2 mM NADH, pH 7.4 PBS buffer, 10 mW cm^{-2} 585 nm orange LED for 60 min. GFP (PDB:1EMG), KillerRed (PDB: 2WIQ), GluER (PDB:6O08), OPR1 (PDB: 1ICQ), YqjM (PDB: 1Z48), iLOV (PDB: 4EES), miniSOG (PDB: 6GPU).

photosensitive proteins (Figure 2a), including: i) fluorescent proteins (e.g., GFP), which are biocompatible but optimized for light emission rather than catalysis;[39] ii) existing artificial photoenzymes (e.g., GluER) designed for in vitro asymmetric synthesis;[40] and iii) optogenetic proteins such as LOV domain flavoproteins, which are compact tools with potential for repurposing into catalysts.

We quantified deboronative hydroxylation activity by measuring the conversion of *p*-boronic ester benzyl alcohol (**1**) to hydroxyl benzyl alcohol (**HBA**) using HPLC

© 2025 Wiley-VCH GmbH

15213773, 2025, 51, Downloaded from https://onlinelibrary.wiley.com/doi/10.1002/anie.202515137 by Shanghai Institute Of Organic Chemistry, Wiley Online Library on [16/12/2025]. See the Terms and Conditions (https://onlinelibrary.wiley.com/terms-and-conditions) on Wiley Online Library for rules of use; OA articles are governed by the applicable Creative Commons License

analysis under standard conditions (ambient O_2, blue light irradiation).[19] As expected, GFP showed minimal activity (7% **HBA** yield), consistent with its inefficient intersystem crossing and lack of photocatalysis reactivity (entry 1, Figure 2a). KillerRed, a Type I photocatalyst, achieved 76% yield via radical-mediated pathways (Table S2) but required higher catalyst and reductant loads (entry 2).[41] Existing artificial photoenzymes (e.g., YqjM, OPR1, and GluER) exhibited high conversion (>95% yield), yet their large molecular sizes (>38 kDa) may hinder subcellular targeting and potentially perturb cellular function in live-cell applications, and their reliance on exogenous cofactors could limit practical use.[42]

LOV domain flavoproteins emerged as promising candidates due to their compact size and genetic encodability. Wild-type LOV proteins achieved good conversion (entry 6) but lacked stability under reaction conditions.[43] We focused on miniSOG, a 12 kDa LOV-derivative with engineered FMN-binding mutations (I1M/N4S/S8T/S26G/C40G/F84L), which outperformed all candidates with > 95% **HBA** yield under ambient O_2 (entry 7).[44] miniSOG also demonstrated superior photostability, retaining nearly 90% fluorescence after 30 min of mild blue light irradiation (6 mW cm^{-2}), compared to 71% for iLOV (Figure S1). Structural analysis suggested that mutations near miniSOG's FMN-binding site disrupt native conformational switching, instead favoring flavin-mediated electron transfer to O_2, resulting in efficient $O_2^{\bullet-}$ generation. This repurposing enables miniSOG to act as a stable $O_2^{\bullet-}$ source with broad catalytic promiscuity.

miniSOG exhibits high catalytic efficiency, achieving > 95% conversion of *p*-boronic ester benzyl alcohol **1** at low loadings (0.05–0.3 mol%) with turnover numbers exceeding 1000 (Figure S2A), outperforming small-molecule analogues and SNAP-tag fusions (Table S4). It retains full activity in complex biomolecular environments (e.g., E. coli lysate, 95% yield) and operates under physiological conditions through synergistic electron transfer and reductant recycling (e.g., via GSH/NADH pathways).[45,46] For detailed mechanistic studies, including UV–vis spectroscopy, scavenger assays, and kinetic analyses, see Figures S2–S4.

miniSOG's selection is based on three synergistic attributes: i) It facilitates deboronative hydroxylation via $O_2^{\bullet-}$ generation (Type I photocatalysis), which is ideal for aerobic environments and avoids self-inactivation common with singlet oxygen ($^1O_2$)-mediated pathways; ii) it maintains excellent photostability under mild irradiation conditions, ensuring sustained activity; and iii) it functions without exogenous cofactors, leveraging endogenous FMN for straightforward genetic encoding and expression in cells. Control experiments confirmed that both miniSOG and blue light irradiation are essential for deboronative hydroxylation (Table S1), underscoring its reliability as a photoenzymatic tool.

Substrate Scope of Organoboronates by miniSOG

To evaluate miniSOG's catalytic versatility for bioorthogonal applications, we designed a library of 27 organoboronates encompassing fluorescent probes, bioactive molecules, and prodrugs using two synthetic strategies (Figure 2b): i) direct replacement of hydroxyl (—OH) groups with boronate esters for phenolic derivatives;[47] ii) self-immolative boronate benzyl linkers conjugated to functional groups (—OH, —COOH, $—NH_2$, or $—CONH_2$) via ether, carbonate, or carbamate spacers to facilitate release of diverse bioactive compounds.[48,49] This approach allowed assessment of miniSOG's ability to facilitate deboronative hydroxylation across broad substrates under physiological conditions.

Simple benzyl boronates (**1–7**) with diverse substitution patterns (e.g., *ortho*-hydroxymethyl, trifluoromethyl, methoxy) achieved 75–95% yields, demonstrating tolerance to steric and electronic perturbations.[50] Notably, alkyl and benzyl boronates (**8–9**), historically challenging for deboronative hydroxylation, underwent efficient conversion (77–95% yields), underscoring miniSOG's capability to generate aliphatic alcohols via $O_2^{\bullet-}$-mediated mechanisms. Caged-fluorogenic substrates (**10–12, 23–24**) validated imaging compatibility: resorufin/diethylrhodol (**10–11**) gave moderate yields (36–51%) due to poor aqueous solubility but remained suitable for cellular tracking; doubly-boronated fluorescein (**12**) showed sequential uncaging (16% total yield), confirming multisite activation; and coumarins (**23–24**) afforded high yields (81–90%), ideal for real-time monitoring in live cells.

To underscore therapeutic potential, we expanded the scope to boronate-caged drug molecules (**13–22, 25–27**). miniSOG facilitated efficient release of 15 bioactive compounds with high yields and specificity: Anti-inflammatory/lipid regulators (**13–15**) afforded > 95% yield (e.g., indomethacin, fenofibrate); mitochondrial uncouplers (**16**) gave > 95% yield release of 2,4-dinitrophenol (**DNP**) for metabolic studies; Ca^{2+}-dependent depolarizer (**17**) released abscisic acid in 95% yield; Anticancer agents (**18, 20**) resulted in > 95% yield uncaging of 5-fluorouracil and 23% for doxorubicin, highlighting cancer therapy potential; $GABA_B$ receptor inhibitor (**19**) showed > 95% yield for baclofen, indicating neurological research applicability. Four epigenetically active substrates achieved efficient activation (81–95% yields), including m^6A methylation agonists (**21–22**) for RNA studies,[51] and DNA/histone modifiers like Procaine (DNA demethylation) and CI-994 (HDAC inhibition) (**25–26**). Notably, caged PARP inhibitor benzamide (**27**) was uncaged with 95% efficiency at its active amide site, demonstrating miniSOG's handling of complex drug motifs. These results highlight miniSOG as a versatile tool for studying RNA epigenetics and cancer biology with high precision.

miniSOG Facilitates Organoboronate Uncaging in Live Cells via Superoxide-Mediated Mechanism

To validate miniSOG's biocompatibility under operational conditions, we rigorously characterized its interactions with biomolecules during catalysis.[52–54] Oxidation-sensitive residues (Cys, Met, Trp) and nucleosides retained > 95% integrity post-irradiation (HPLC, Table S3). Bovine serum albumin showed no detectable degradation after 30 min

© 2025 Wiley-VCH GmbH

15213773, 2025, 51, Downloaded from https://onlinelibrary.wiley.com/doi/10.1002/anie.202515137 by Shanghai Institute Of Organic Chemistry, Wiley Online Library on [16/12/2025]. See the Terms and Conditions (https://onlinelibrary.wiley.com/terms-and-conditions) on Wiley Online Library for rules of use; OA articles are governed by the applicable Creative Commons License

illumination (4 mW cm^{-2}) (CBB staining, Figure S5A), demonstrating that under these conditions, miniSOG maintains sufficient biocompatibility for catalytic applications. DNA fragments (318 bp) maintain structural integrity after 30 min illumination (agarose gel, Figure S5A), consistent with its minimal singlet oxygen quantum yield ($\Phi_\Delta \approx 0.03$).[55–57] Under mild blue light irradiation (6 mW cm^{-2}), $O_2^{\bullet-}$ generation was dominant, with negligible singlet oxygen ($^1O_2$) production[25]—aligning with SNAP-FL benchmarks and contrasting with high-intensity applications (e.g., photocatalytic labeling or CALI at 30–10,000 mW cm^{-2}, Figure 3a, left).[35,58,59] This selectivity arises from low light intensity ($\leq$6 mW cm^{-2}) and short irradiation times ($\leq$10 min for live-cell applications), which minimize cumulative phototoxicity (Figure S6A), as supported by prior studies on flavin-mediated superoxide generation. Increasing light intensity (30–10,000 mW cm^{-2}) enhances both ROS formation, with $^1O_2$ levels becoming cytotoxic, underscoring the importance of controlled operational parameters for biocompatibility.

The miniSOG protein scaffold suppresses singlet oxygen generation compared to free flavins (Φ_Δ ~0.5; Figures S3A and S5B), which, combined with short irradiation protocols, enables spatially controlled catalysis without significant collateral damage (Figure S6A). This biocompatibility was evident across diverse cell lines, with >90% viability maintained in HeLa, HEK293T, HT22, and MCF-7 cells (MTT, Figures 3a and S6B), a result in sharp contrast to the cytotoxicity observed under CALI conditions. No oxidative collateral damage was detected: transcriptional stress responses remained unchanged (Figure S6C), and off-target labeling was absent (western blot, Figure S7A).[60] Functional assays confirmed preserved mitochondrial membrane potential ($\Delta\psi_m$) and no impairment (Figure S6D, right). Targeting miniSOG to specific organelles (mitochondria, nucleus, or cytosol) in HeLa cells resulted in > 90% viability post-irradiation (MTT assay, Figure S7B), confirming compatibility even under spatial constraints.

We next assessed miniSOG's photoenzymatic efficacy and spatiotemporal control in live cells (Figure 3b). miniSOG mediates deboronative hydroxylation of organoboronates via $O_2^{\bullet-}$ generation, leading to uncaging events such as the conversion of AMC-Bpin (**23**) to fluorescent 7-amino-4-methylcoumarin (**AMC**). This reaction enables direct visualization of catalytic efficiency and subcellular localization. In vitro, miniSOG achieved 90% uncaging efficiency for AMC-Bpin (**23**) (Figure S9). In HeLa cells expressing miniSOG, robust **AMC** fluorescence was observed within 10 min of irradiation, demonstrating efficient intracellular photocatalysis under biological conditions (Figure 3b, top panel).

Fluorescence colocalization imaging with organelle trackers confirmed precise spatial localization of miniSOG in both the nucleus and mitochondria (Figure S8). For organelle-specific modulation, mitochondria-targeted miniSOG (mito-miniSOG) showed **AMC** signal colocalization with mitochondria, while nucleus-targeted miniSOG (NLS-miniSOG) confined uncaging to the nucleus, as evidenced by line profile overlays (Figure 3b, lower panel). Controls exhibited minimal background (<5% **AMC** signal in miniSOG-free cells or dark conditions, Figure S10). Unlike systems requiring exogenous components, miniSOG operates as a genetically encoded photocatalyst without washing steps, enabling sustained in situ activity (Figure S11). This design results in superior performance: >12 × higher uncaging efficiency and > 12 × fluorescence contrast compared to SNAP-tag systems (Figure 3c)

miniSOG Enables Spatiotemporally Controlled Mitochondrial Uncoupling

Building on the demonstrated effectiveness of our photoenzymatic method, we applied it to modulate cellular function with spatiotemporal precision. Mitochondrial uncoupling via 2,4-dinitrophenol (**DNP**) offers therapeutic potential for metabolic disorders such as NAFLD and obesity, but its clinical translation is limited by systemic toxicity.[61,62] Localized **DNP** release could mitigate metabolic dysfunction without systemic effects, necessitating strategies that combine dose control and subcellular targeting to enhance therapeutic specificity.[63] While prior studies have achieved either dose precision or mitochondrial targeting of **DNP** release,[64,65] achieving both at the same time has not been achieved.

To address this, we engineered a mitochondria-targeted miniSOG system (mito-miniSOG) to enable localized **DNP** release from a boronate-caged prodrug (DNP-Bpin, **16**) (Figure 4a). This approach integrates key design principles: subcellular precision (via mitochondrial targeting sequences), temporal control (light-gated uncaging), and bioorthogonality ($O_2^{\bullet-}$-mediated deboronative hydroxylation without perturbing endogenous pathways). miniSOG photocatalytically generates $O_2^{\bullet-}$ under blue light, which then diffuses and mediates the deboronative hydroxylation of DNP-Bpin, ensuring confined reactivity.

In vitro validation confirmed that miniSOG facilitates uncaging of DNP-Bpin with 95% efficiency under ambient O_2 conditions (HPLC, Figure S12), demonstrating robust catalytic performance. In HeLa cells, we quantified mitochondrial depolarization using tetramethylrhodamine ethyl ester (TMRE) as a $\Delta\psi_m$-sensitive dye.[66] Spatially targeted photocatalysis with mito-miniSOG triggered rapid and significant mitochondrial depolarization (>70% loss of $\Delta\psi_m$) within 5 min of mild blue-light irradiation (Figure 4b). This effect was strictly dependent on mitochondrial localization as cytosolic miniSOG failed to induce $\Delta\psi_m$ loss under identical conditions (Figure 4b), highlighting the system's spatial precision. Control experiments confirmed no depolarization with DNP-Bpin alone or light irradiation alone (Figure S13A).

The photoenzymatic approach enables precise titration of the depolarization response. Mitochondrial membrane potential loss ($\Delta\psi_m$) scaled linearly with irradiation duration (0–10 min, $R^2 = 0.99$) (Figure S13B). Mito-miniSOG-mediated uncaging of 10 μM DNP-Bpin induced near-complete depolarization (80% $\Delta\psi_m$ loss), equivalent to 10 μM FCCP (78% $\Delta\psi_m$ loss; Figure 4c). Even at 1 μM DNP-Bpin, significant depolarization (54%) was achieved (Figure 4d).[67] Importantly, targeted activation with 10 μM DNP-Bpin maintained high cell viability (94%; Figure S13D) and demonstrated superior depolarization efficiency compared to systemic **DNP**

© 2025 Wiley-VCH GmbH

15213773, 2025, 51, Downloaded from https://onlinelibrary.wiley.com/doi/10.1002/anie.202515137 by Shanghai Institute Of Organic Chemistry, Wiley Online Library on [16/12/2025]. See the Terms and Conditions (https://onlinelibrary.wiley.com/terms-and-conditions) on Wiley Online Library for rules of use; OA articles are governed by the applicable Creative Commons License

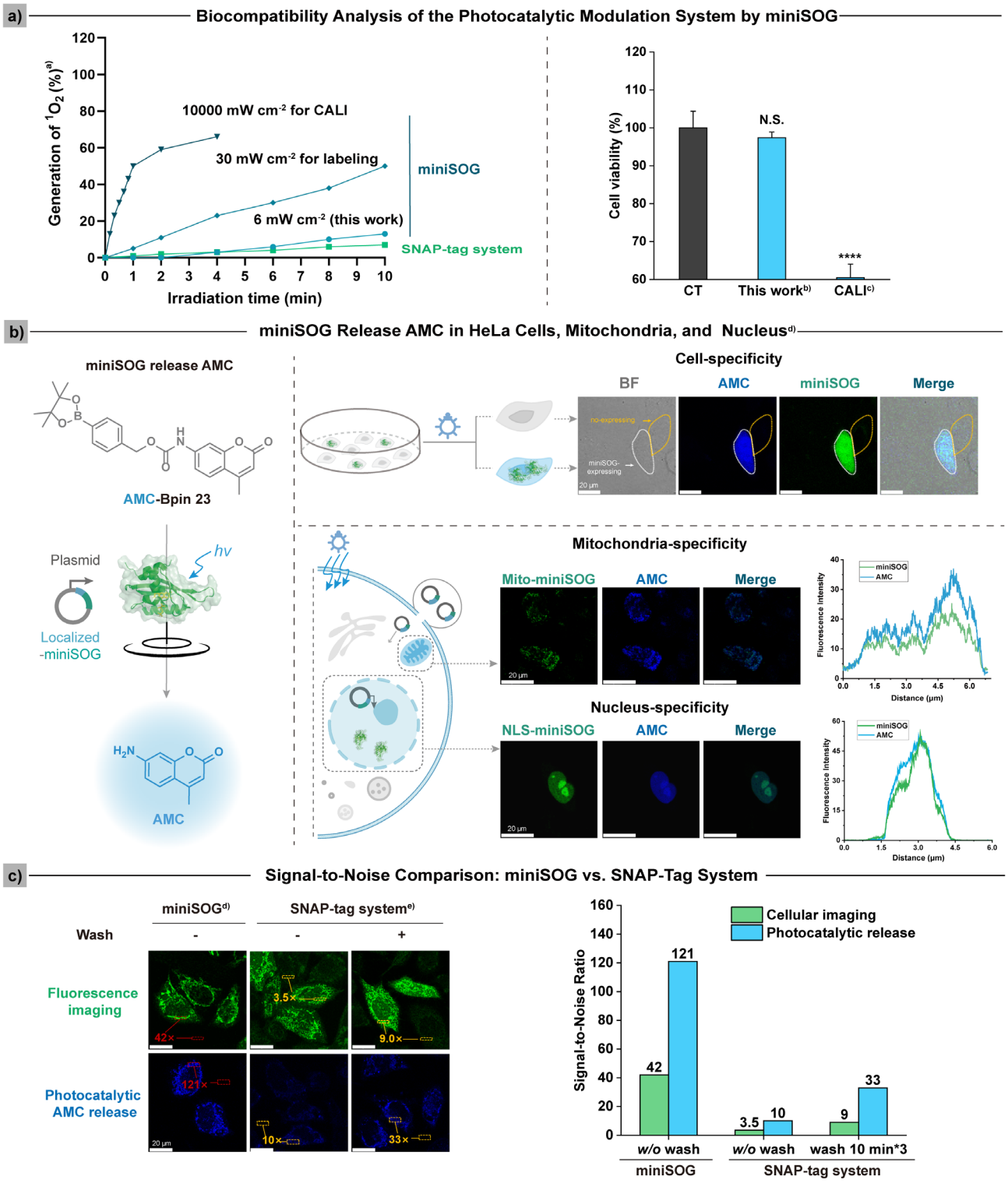

Figure 3. miniSOG enables deboronative hydroxylation with biomolecule-compatibility and in live cells. a) Biocompatibility analysis of the photocatalytic system by miniSOG. Cell viability was assessed using the MTT assay. Data were normalized to the without light control group, which was set as 100%. Values represent mean ± S.E.M. ($n = 3$). Statistical significance was determined using an unpaired two-tailed Student's t-test (N.S., no significant difference, ****$p < 0.0001$). b) miniSOG releases **AMC** in HeLa cells, mitochondria, and the nucleus. White dashed circles: miniSOG-expressing cells. Orange dashed circles: Non-miniSOG-expressing cells. c) Signal-to-noise comparison of miniSOG and SNAP-tag system. Scale bars: 20 μm. [a] Reaction conditions: 2 μM miniSOG or SNAP-FL, 50 μM uric acid, pH 7.4 PBS buffer, blue LED irradiation for various durations. [b] 6 mW cm^{-2} blue LED 10 min irradiation. [c] 10000 mW cm^{-2} blue LED 30 min. [d] Standard reaction conditions: 20 μM AMC-Bpin (**23**), pH 7.4 HBSS buffer, 19 mW cm^{-2} blue LED 10 min. [e] with or without (*w/o*) wash by PBS (10 min*3), under otherwise standard reaction conditions.

© 2025 Wiley-VCH GmbH

15213773, 2025, 51, Downloaded from https://onlinelibrary.wiley.com/doi/10.1002/anie.202515137 by Shanghai Institute Of Organic Chemistry, Wiley Online Library on [16/12/2025]. See the Terms and Conditions (https://onlinelibrary.wiley.com/terms-and-conditions) on Wiley Online Library for rules of use; OA articles are governed by the applicable Creative Commons License

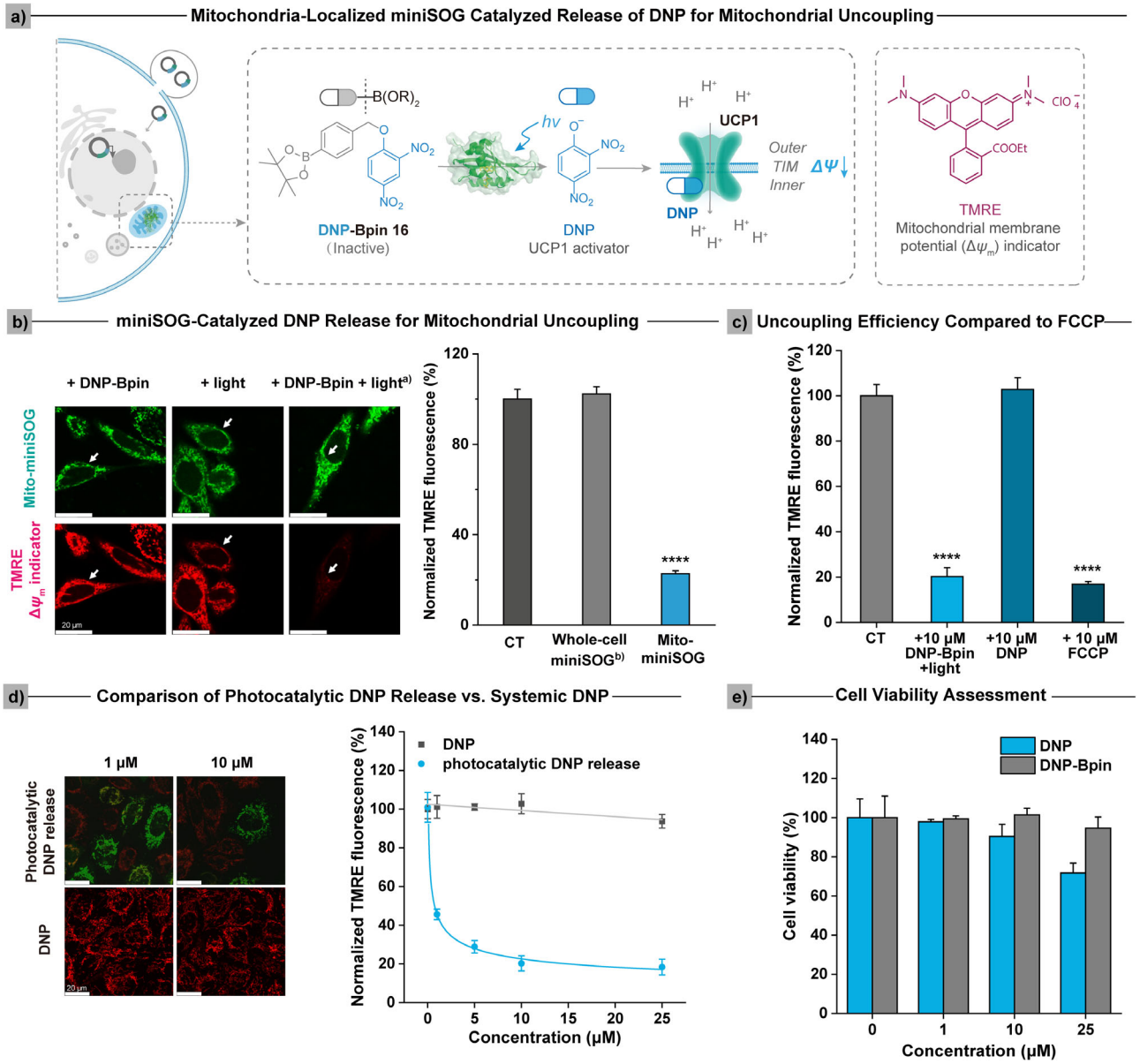

Figure 4. miniSOG-catalysis induces mitochondrial uncoupling via DNP release. a) Mitochondria-localized release of DNP for mitochondrial uncoupling. b) DNP release modulates mitochondrial inner membrane potential. Scale bars: 20 μm. Values represent mean ± S.E.M. ($n = 9$). c) Comparison of uncoupling efficiency: DNP release via miniSOG versus FCCP ($n = 5$). d) Comparison of photocatalytic DNP release versus systemic DNP ($n = 5$). e) Cell viability assessment of DNP and DNP-Bpin. Cell viability was assessed using the MTT assay. Data were normalized to the DMSO-only control group, which was set as 100% ($n = 3$). Statistical significance was determined using an unpaired two-tailed Student's t-test (****$p < 0.0001$). [a)] Standard reaction conditions: HeLa cells transfected with mito-miniSOG, 10 μM DNP-Bpin (**16**), 6 mW cm^{-2} blue LED 5 min, 1 μM TMRE. [b)] HeLa cells transfected with whole-cell miniSOG.

exposure, which at 25 μM caused ~30% cell death (MTT; Figure 4e) with only moderate depolarization (36% $\Delta\psi_m$ loss at 24 h; Figure S13C). This underscores the potential of miniSOG for safe and effective mitochondrial modulation.

Spatiotemporal Control of m^{6}A Methylation via miniSOG Catalysis

N^6-methyladenosine (m^6A) dynamically regulates RNA metabolism and is implicated in diseases ranging from cancer to neurodegeneration.[68] Developing methods to modulate m^6A with high spatiotemporal precision is thus paramount. While CRISPR-based m^6A editing tools offer targeted manipulation, they often lack temporal control and can disrupt endogenous methylation balance.[69] Opto-chemical uncaging strategies provide an alternative but may suffer from limited subcellular specificity.[70,71] To address these challenges, we leveraged miniSOG's genetic encodability and $O_2^{\bullet-}$-driven deboronative hydroxylation to achieve light-gated, organelle-specific m^6A modulation (Figure 5a).

© 2025 Wiley-VCH GmbH

15213773, 2025, 51, Downloaded from https://onlinelibrary.wiley.com/doi/10.1002/anie.202515137 by Shanghai Institute Of Organic Chemistry, Wiley Online Library on [16/12/2025]. See the Terms and Conditions (https://onlinelibrary.wiley.com/terms-and-conditions) on Wiley Online Library for rules of use; OA articles are governed by the applicable Creative Commons License

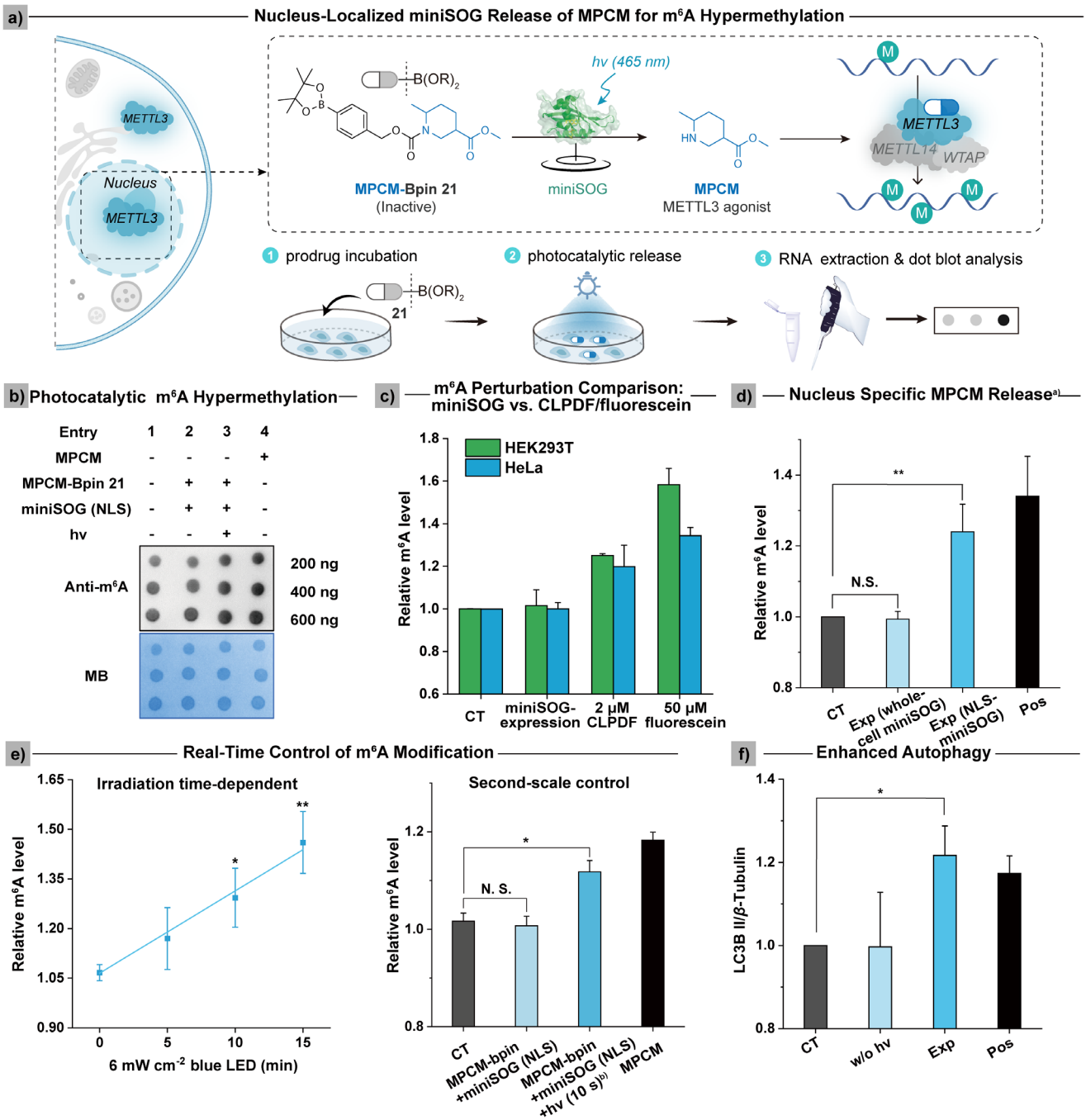

Figure 5. miniSOG catalyzed release of METTL3 agonist induces m^{6}A hypermethylation. a) Nucleus-localized miniSOG release of **MPCM** for m^{6}A hypermethylation. b) miniSOG catalysis enables **MPCM** release to modulate m^{6}A methylation. Standard reaction conditions: HEK 293T cells transfected with NLS-miniSOG, 1 μM MPCM-Bpin (**21**), 6 mW cm^{-2} blue LED 5 min. The uncropped blot and gel are shown in Figure S20. c) Cellular m^{6}A perturbation comparison: miniSOG versus organic dye and SNAP-tag system. The raw data and uncropped blot/gel images are shown in Figure S6 and Figure S21, respectively. d) m^{6}A hypermethylation with nucleus-specific **MPCM** release. The raw data and uncropped blot/gel images are shown in Table S7 and Figure S22, respectively. e) Irradiation-dependent real-time control of m^{6}A modification. The raw data and uncropped blot/gel images are shown in Table S8, S9 and Figures S23, S24, respectively. f) Enhanced autophagy following m^{6}A hypermethylation via nucleus-specific **MPCM** release. The raw data and uncropped blot/gel images are shown in Table S10 and Figure S25, respectively. Values represent mean ± S.E.M. ($n = 3$). Statistical significance was determined using an unpaired two-tailed Student's t-test (N.S., no significant difference, *$p < 0.05$, **$p < 0.01$). [a]Whole represents whole-cell miniSOG; NLS represents NLS-miniSOG; Pos (positive control) represents HeLa cells with 2 μM MPCM incubation, CT represents the DMSO-only control group. [b]20 mW mm^{-2} blue LED 10 s.

© 2025 Wiley-VCH GmbH

15213773, 2025, 51, Downloaded from https://onlinelibrary.wiley.com/doi/10.1002/anie.202515137 by Shanghai Institute Of Organic Chemistry, Wiley Online Library on [16/12/2025]. See the Terms and Conditions (https://onlinelibrary.wiley.com/terms-and-conditions) on Wiley Online Library for rules of use; OA articles are governed by the applicable Creative Commons License

6-Methyl-3-piperidinecarboxylic acid methyl ester (**MPCM**) is a known agonist of the METTL3/METTL14/WTAP complex.[51] We engineered a boronate-caged **MPCM** prodrug (MPCM-Bpin, **21**) to block its bioactivity until uncaging. In vitro, miniSOG (10 μM) achieved near-quantitative release (>95%) of **MPCM** within 10 min under blue light illumination (HPLC quantification; Figure S14). In HEK 293T cells, MPCM-Bpin **21** (50 μM) alone induced negligible m^{6}A methylation (Figure S15A), confirming effective caging. Upon irradiation, cells expressing nucleus-targeted miniSOG (NLS-miniSOG) showed significant m^{6}A upregulation (Dot blot, Figure 5b), demonstrating successful light-gated activation.

Unlike platforms relying on exogenous photosensitizers or SNAP-tag fusions, miniSOG's genetically encoded architecture avoids cellular artifacts inherent to additive-based approaches. Exogenous catalysts can perturb key pathways: fluorescein dyes may inhibit m^{6}A demethylase FTO, causing aberrant methylation (Figure 5c),[72] while SNAP-tag ligands CLPDF may suppress alkylguanine-DNA alkyltransferase (Figure S16).[20] In contrast, miniSOG expression preserves endogenous biomolecular landscapes—transcriptional stress markers (Figure S6C) and METTL3 stability (Figure S6D, left) remain unchanged post-illumination—ensuring uncaging proceeds without artificial perturbation.

To validate spatial control, we compared m^{6}A levels in cells expressing nucleus-targeted, unlocalized, or mitochondria-targeted miniSOG. Nucleus-targeted miniSOG induced a 1.20-fold m^{6}A upregulation, while unlocalized and mitochondrial variants showed no significant change, consistent with METTL3's nuclear localization (Figures 5d and S15B). This upregulation persisted at low MPCM-Bpin **21** concentrations (0.5 μM, Figure S15C), matching positive controls (Figure S15D) with minimal background (Figures S15E,F) and >90% cell viability (Figure S15G). This represents the first demonstration of nucleus-targeted photocatalytic m^{6}A modulation, enabling precise study of RNA regulation without overexpression-induced imbalances.

miniSOG's genetic encoding enables continuous, titratable photocatalysis—unattainable with transient small-molecule photosensitizers. Constitutive expression sustains activity without depletion, allowing real-time manipulation. This is quantified by linear irradiation-time-dependent m^{6}A accumulation (R^2 = 0.99; 0–15 min, Figure 5e, left) and robust responsiveness to 10-s irradiation (20 mW mm^{-2}) with negligible phototoxicity (>95% viability, Figure 5e, right, Figure S15H). This combination of longitudinal activity and dosage control facilitates perturbation of transient biological processes.

Aberrant m^{6}A-autophagy crosstalk is implicated in cancer[73,74] prompting us to investigate downstream effects. **MPCM** activation of METTL3/METTL14/WTAP complex elevated m^{6}A methylation (Figure S17A), which enhanced autophagy flux—measured by LC3-II accumulation (1.2-fold versus control, $p < 0.05$, Figure S17B) in the presence of bafilomycin A1. Light-triggered MPCM-Bpin **21** uncaging further increased LC3-II levels by 1.28-fold ($p < 0.05$, Figures 5f and S17C), following m^{6}A hypermethylation. No changes occurred without light, miniSOG, or prodrug **21** (Figure S17D), excluding off-target effects.[75] To demonstrate versatility, we tested MPCH-Bpin (**22**), a boronate-caged METTL3 agonist with sub-nM EC_{50} (109 pM). miniSOG achieved 83% uncaging in vitro (HPLC, Figure S18) and induced comparable m^{6}A upregulation (1.3-fold, ~60% of systemic **MPCH**, $p < 0.001$, Figure S19) in cells, confirming its broad applicability for epitranscriptomic studies.

Conclusion

In conclusion, we have established miniSOG as a genetically encoded miniature photoenzyme that facilitates bioorthogonal deboronative hydroxylation via $O_2^{\bullet-}$ generation, achieving unparalleled spatiotemporal precision in live cells. By leveraging its endogenous expression and compact size (12 kDa), miniSOG delivers three foundational advances: 1) elimination of unbound catalyst background through genetic encoding, ensuring high signal-to-noise ratios without exogenous components; 2) minimal cellular perturbation, maintaining homeostasis (>90% viability under standard conditions) and avoiding artifacts associated with exogenous photocatalysts; and 3) continuous, real-time modulation without washing steps, enabling dose-titratable responses down to 10-s irradiation for dynamic biological interrogation.

The spatial confinement of reactivity (~0.2 μm diffusion radius) arises from rapid $O_2^{\bullet-}$ quenching by endogenous reductants (e.g., GSH, NADH), permitting precise organelle-specific modulation—demonstrated in targeted mitochondrial depolarization (94% viability), nuclear m^{6}A hypermethylation (1.2-fold increase), and enhanced autophagy. By seamlessly integrating optogenetic precision with enzymatic efficiency, miniSOG provides a biocompatible, genetically embedded platform for perturbing intracellular dynamics—such as energy metabolism and epigenetic regulation—in physiologically intact environments.

Acknowledgements

Financial support was provided by the National Natural Science Foundation of China 22337005, 22277133, the Strategic Priority Research Program of the Chinese Academy of Sciences XDB1060000, Youth Innovation Promotion Association CAS 2023266, Shanghai Oriental Talent Leadership Program, and International Partnership Program of the Chinese Academy of Science 033GJHZ2023006FN. Some figures were created with Biorender.com.

Conflict of Interests

The authors declare no conflict of interest.

Data Availability Statement

The data that support the findings of this study are available in the Supporting Information of this article.

© 2025 Wiley-VCH GmbH

15213773, 2025, 51, Downloaded from https://onlinelibrary.wiley.com/doi/10.1002/anie.202515137 by Shanghai Institute Of Organic Chemistry, Wiley Online Library on [16/12/2025]. See the Terms and Conditions (https://onlinelibrary.wiley.com/terms-and-conditions) on Wiley Online Library for rules of use; OA articles are governed by the applicable Creative Commons License

Keywords: Bioorthogonal reaction • Organelle-specific • Organoboronates • Photocatalytic uncaging • Photoenzymes

[1] M. A. Emmanuel, S. G. Bender, C. Bilodeau, J. M. Carceller, J. S. DeHovitz, H. Fu, Y. Liu, B. T. Nicholls, Y. Ouyang, C. G. Page, T. Qiao, F. C. Raps, D. R. Sorigué, S.-Z. Sun, J. Turek-Herman, Y. Ye, A. Rivas-Souchet, J. Cao, T. K. Hyster, *Chem. Rev.* **2023**, *123*, 5459–5520, https://doi.org/10.1021/acs.chemrev.2c00767.

[2] E. N. Kissman, M. B. Sosa, D. C. Millar, E. J. Koleski, K. Thevasundaram, M. C. Y. Chang, *Nature* **2024**, *631*, 37–48, https://doi.org/10.1038/s41586-024-07506-w.

[3] M. A. Emmanuel, N. R. Greenberg, D. G. Oblinsky, T. K. Hyster, *Nature* **2016**, *540*, 414–417, https://doi.org/10.1038/nature20569.

[4] X. Huang, B. Wang, Y. Wang, G. Jiang, J. Feng, H. Zhao, *Nature* **2020**, *584*, 69–74, https://doi.org/10.1038/s41586-020-2406-6.

[5] Z. C. Litman, Y. Wang, H. Zhao, J. F. Hartwig, *Nature* **2018**, *560*, 355–359, https://doi.org/10.1038/s41586-018-0413-7.

[6] Y. Xu, H. Chen, L. Yu, X. Peng, J. Zhang, Z. Xing, Y. Bao, A. Liu, Y. Zhao, C. Tian, Y. Liang, X. Huang, *Nature* **2024**, *625*, 74–78, https://doi.org/10.1038/s41586-023-06822-x.

[7] E. M. Sletten, C. R. Bertozzi, *Angew. Chem. Int. Ed.* **2009**, *48*, 6974–6998, https://doi.org/10.1002/anie.200900942.

[8] M. Mato, X. Fernández-González, C. D'Avino, M. Tomás-Gamasa, J. L. Mascareñas, *Angew. Chem. Int. Ed.* **2024**, *63*, e202413506, https://doi.org/10.1002/anie.202413506.

[9] K. Chen, F. H. Arnold, *Nat. Catal.* **2020**, *3*, 203–213, https://doi.org/10.1038/s41929-019-0385-5.

[10] S. L. Lovelock, R. Crawshaw, S. Basler, C. Levy, D. Baker, D. Hilvert, A. P. Green, *Nature* **2022**, *606*, 49–58, https://doi.org/10.1038/s41586-022-04456-z.

[11] A. Losi, K. H. Gardner, A. Möglich, *Chem. Rev.* **2018**, *118*, 10659–10709, https://doi.org/10.1021/acs.chemrev.8b00163.

[12] V. Emiliani, E. Entcheva, R. Hedrich, P. Hegemann, K. R. Konrad, C. Lüscher, M. Mahn, Z.-H. Pan, R. R. Sims, J. Vierock, O. Yizhar, *Nat. Rev. Methods Primers* **2022**, *2*, 55, https://doi.org/10.1038/s43586-022-00136-4.

[13] K. Hüll, J. Morstein, D. Trauner, *Chem. Rev.* **2018**, *118*, 10710–10747;

[14] N. Ankenbruck, T. Courtney, Y. Naro, A. Deiters, *Angew. Chem. Int. Ed.* **2018**, *57*, 2768–2798, https://doi.org/10.1002/anie.201700171.

[15] H. Wang, Y. Zhang, K. Zeng, J. Qiang, Y. Cao, Y. Li, Y. Fang, Y. Zhang, Y. Chen, *JACS Au* **2021**, *1*, 1066–1075;

[16] X. Chen, R. He, H. Xiong, R. Wang, Y. Yin, Y. Chen, Z. Zhu, *Nat. Chem.* **2025**, *17*, 1534–1545, https://doi.org/10.1038/s41557-025-01886-w.

[17] A. R. Lippert, G. C. Van de Bittner, C. J. Chang, *Acc. Chem. Res.* **2011**, *44*, 793–804, https://doi.org/10.1021/ar200126t.

[18] R. J. Grams, W. L. Santos, I. R. Scorei, A. Abad-García, C. A. Rosenblum, A. Bita, H. Cerecetto, C. Viñas, M. A. Soriano-Ursúa, *Chem. Rev.* **2024**, *124*, 2441–2511, https://doi.org/10.1021/acs.chemrev.3c00663.

[19] H. Wang, W. G. Li, K. Zeng, Y. J. Wu, Y. Zhang, T. L. Xu, Y. Chen, *Angew. Chem. Int. Ed.* **2019**, *58*, 561–565, https://doi.org/10.1002/anie.201811261.

[20] A. Keppler, S. Gendreizig, T. Gronemeyer, H. Pick, H. Vogel, K. Johnsson, *Nat. Biotechnol.* **2003**, *21*, 86–89, https://doi.org/10.1038/nbt765.

[21] K. Zeng, Z.-H. Jiao, Q. Jiang, R. He, Y. Zhang, W.-G. Li, T.-L. Xu, Y. Chen, *ACS Cent. Sci.* **2024**, *10*, 163–175, https://doi.org/10.1021/acscentsci.3c01351.

[22] Y. Zhang, L. Han, X. Tian, C. Peng, Y. Chen, *Angew. Chem. Int. Ed.* **2022**, *61*, e202115472, https://doi.org/10.1002/anie.202115472.

[23] L. Wang, M. Tran, E. D'Este, J. Roberti, B. Koch, L. Xue, K. Johnsson, *Nat. Chem.* **2020**, *12*, 165–172, https://doi.org/10.1038/s41557-019-0371-1.

[24] M. Minoshima, S. I. Reja, R. Hashimoto, K. Iijima, K. Kikuchi, *Chem. Rev.* **2024**, *124*, 6198–6270, https://doi.org/10.1021/acs.chemrev.3c00549.

[25] X. Shu, V. Lev-Ram, T. J. Deerinck, Y. Qi, E. B. Ramko, M. W. Davidson, Y. Jin, M. H. Ellisman, R. Y. Tsien, *PLoS Biol.* **2011**, *9*, e1001041, https://doi.org/10.1371/journal.pbio.1001041.

[26] P. F. Heelis, *Chem. Soc. Rev.* **1982**, *11*, 15–39, https://doi.org/10.1039/cs9821100015.

[27] D. Ballou, G. Palmer, V. Massey, *Biochem. Biophys. Res. Commun.* **1969**, *36*, 898–904, https://doi.org/10.1016/0006-291X(69)90288-5.

[28] M. Korycka-Dahl, T. Richardson, *J. Dairy Sci.* **1978**, *61*, 400–407, https://doi.org/10.3168/jds.S0022-0302(78)83613-3.

[29] J.-Y. Liang, C.-W. Cheng, C.-H. Yu, L.-Y. Chen, *J. Photochem. Photobiol. B* **2015**, *143*, 82–88, https://doi.org/10.1016/j.jphotobiol.2015.01.005.

[30] M. E. Barnett, T. M. Baran, T. H. Foster, A. P. Wojtovich, *Free Radical Biol. Med.* **2018**, *116*, 134–140, https://doi.org/10.1016/j.freeradbiomed.2018.01.014.

[31] J. Torra, C. Lafaye, L. Signor, S. Aumonier, C. Flors, X. Shu, S. Nonell, G. Gotthard, A. Royant, *Sci. Rep.* **2019**, *9*, 2428.

[32] Y. Q. Zou, J. R. Chen, X. P. Liu, L. Q. Lu, R. L. Davis, K. A. Jørgensen, W. J. Xiao, *Angew. Chem. Int. Ed.* **2012**, *124*, 808–812, https://doi.org/10.1002/ange.201107028.

[33] S. P. Pitre, C. D. McTiernan, H. Ismaili, J. C. Scaiano, *J. Am. Chem. Soc.* **2013**, *135*, 13286–13289, https://doi.org/10.1021/ja406311g.

[34] M. Liu, Y. Luo, J. Yan, X. Xiong, X. Xing, J. S. Kim, T. Zou, *J. Am. Chem. Soc.* **2023**, *145*, 10082–10091, https://doi.org/10.1021/jacs.3c00254.

[35] J. Y. Lin, S. B. Sann, K. Zhou, S. Nabavi, C. D. Proulx, R. Malinow, Y. Jin, R. Y. Tsien, *Neuron* **2013**, *79*, 241–253, https://doi.org/10.1016/j.neuron.2013.05.022.

[36] T.-L. To, K. F. Medzihradszky, A. L. Burlingame, W. F. DeGrado, H. Jo, X. Shu, *Bioorg. Med. Chem. Lett* **2016**, *26*, 3359–3363, https://doi.org/10.1016/j.bmcl.2016.05.034.

[37] P. Wang, W. Tang, Z. Li, Z. Zou, Y. Zhou, R. Li, T. Xiong, J. Wang, P. Zou, *Nat. Chem. Biol.* **2019**, *15*, 1110–1119, https://doi.org/10.1038/s41589-019-0368-5.

[38] X. Xie, Y. Jiang, C. J. Chang, *Proc. Natl. Acad. Sci* **2023**, *120*, e2305211120.

[39] M. Wang, Y. Da, Y. Tian, *Chem. Soc. Rev.* **2023**, *52*, 1189–1214, https://doi.org/10.1039/D2CS00419D.

[40] S. Zhang, S. Liu, Y. Sun, S. Li, J. Shi, Z. Jiang, *Chem. Soc. Rev.* **2021**, *50*, 13449–13466, https://doi.org/10.1039/D1CS00392E.

[41] R. B. Vegh, K. M. Solntsev, M. K. Kuimova, S. Cho, Y. Liang, B. L. Loo, L. M. Tolbert, A. S. Bommarius, *Chem. Commun.* **2011**, *47*, 4887, https://doi.org/10.1039/c0cc05713d.

[42] W. Harrison, X. Huang, H. Zhao, *Acc. Chem. Res.* **2022**, *55*, 1087–1096, https://doi.org/10.1021/acs.accounts.1c00719.

[43] M. D. Hoffmann, F. Bubeck, R. Eils, D. Niopek, *Adv. Biosyst.* **2018**, *2*, 1880098, https://doi.org/10.1002/adbi.201800098.

[44] J. M. Christie, K. Hitomi, A. S. Arvai, K. A. Hartfield, M. Mettlen, A. J. Pratt, J. A. Tainer, E. D. Getzoff, *J. Biol. Chem.* **2012**, *287*, 22295–22304, https://doi.org/10.1074/jbc.M111.318881.

[45] S. Parvez, M. J. C. Long, J. R. Poganik, Y. Aye, *Chem. Rev.* **2018**, *118*, 8798–8888, https://doi.org/10.1021/acs.chemrev.7b00698.

[46] J. B. Lim, B. K. Huang, W. M. Deen, H. D. Sikes, *Free Radical Biol. Med.* **2015**, *89*, 47–53, https://doi.org/10.1016/j.freeradbiomed.2015.07.009.

[47] M. C. Y. Chang, A. Pralle, E. Y. Isacoff, C. J. Chang, *J. Am. Chem. Soc.* **2004**, *126*, 15392–15393, https://doi.org/10.1021/ja0441716.

© 2025 Wiley-VCH GmbH

15213773, 2025, 51, Downloaded from https://onlinelibrary.wiley.com/doi/10.1002/anie.202515137 by Shanghai Institute Of Organic Chemistry, Wiley Online Library on [16/12/2025]. See the Terms and Conditions (https://onlinelibrary.wiley.com/terms-and-conditions) on Wiley Online Library for rules of use; OA articles are governed by the applicable Creative Commons License

[48] J. L. M. Jourden, K. B. Daniel, S. M. Cohen, *Chem. Commun.* **2011**, *47*, 7968, https://doi.org/10.1039/c1cc12526e.
[49] E.-J. Kim, S. Bhuniya, H. Lee, H. M. Kim, C. Cheong, S. Maiti, K. S. Hong, J. S. Kim, *J. Am. Chem. Soc.* **2014**, *136*, 13888–13894, https://doi.org/10.1021/ja5077684.
[50] R. A. Mosey, P. E. Floreancig, *Org. Biomol. Chem.* **2012**, *10*, 7980, https://doi.org/10.1039/c2ob26571k.
[51] S. Selberg, D. Blokhina, M. Aatonen, P. Koivisto, A. Siltanen, E. Mervaala, E. Kankuri, M. Karelson, *Cell Rep.* **2019**, *26*, 3762–3771.e5, https://doi.org/10.1016/j.celrep.2019.02.100.
[52] H. Huang, G. Zhang, L. Gong, S. Zhang, Y. Chen, *J. Am. Chem. Soc.* **2014**, *136*, 2280–2283, https://doi.org/10.1021/ja413208y.
[53] C. Hu, Y. Chen, *Tetrahedron Lett.* **2015**, *56*, 884–888, https://doi.org/10.1016/j.tetlet.2014.12.034.
[54] M. Teders, C. Henkel, L. Anhäuser, F. Strieth-Kalthoff, A. Gómez-Suárez, R. Kleinmans, A. Kahnt, A. Rentmeister, D. Guldi, F. Glorius, *Nat. Chem.* **2018**, *10*, 981–988, https://doi.org/10.1038/s41557-018-0102-z.
[55] R. Ruiz-González, A. L. Cortajarena, S. H. Mejias, M. Agut, S. Nonell, C. Flors, *J. Am. Chem. Soc.* **2013**, *135*, 9564–9567, https://doi.org/10.1021/ja4020524.
[56] Y. Huang, Y. Zhang, C. Hu, Y. Chen, *Org. Chem. Front.* **2024**, *11*, 4408–4415, https://doi.org/10.1039/D4QO00752B.
[57] Y. Zhang, Y. Huang, Q. Che, Y. Chen, *Chin. J. Chem.* **2025**, *43*, 97–103, https://doi.org/10.1002/cjoc.202400796.
[58] T. Ding, L. Zhu, Y. Fang, Y. Liu, W. Tang, P. Zou, *Angew. Chem. Int. Ed.* **2020**, *59*, 22933–22937, https://doi.org/10.1002/anie.202005486.
[59] Y. Zhai, X. Huang, K. Zhang, Y. Huang, Y. Jiang, J. Cui, Z. Zhang, C. K. C. Chiu, W. Zhong, G. Li, *Nat. Commun.* **2022**, *13*, 4906, https://doi.org/10.1038/s41467-022-32689-z.
[60] We observed minimal histidine/deoxyguanosine oxidation under 6 mW/cm^2 blue LED irradiation (HPLC, Fig. S7A).
[61] J. H. Murray, A. L. Burgio, M. Beretta, S. R. Hargett, T. E. Harris, E. Olzomer, R. J. Grams, C. J. Garcia, C. Li, J. M. Salamoun, K. L. Hoehn, W. L. Santos, *J. Med. Chem.* **2023**, *66*, 3876–3895, https://doi.org/10.1021/acs.jmedchem.2c01573.
[62] Y. Kang, L. Chen, *Nature* **2023**, *620*, 226–231, https://doi.org/10.1038/s41586-023-06332-w.
[63] R. Shrestha, E. Johnson, F. L. Byrne, *Mol. Metab.* **2021**, *51*, 101222.
[64] R. J. Perry, D. Zhang, X.-M. Zhang, J. L. Boyer, G. I. Shulman, *Science* **2015**, *347*, 1253–1256, https://doi.org/10.1126/science.aaa0672.
[65] M. Tomás-Gamasa, M. Martínez-Calvo, J. R. Couceiro, J. L. Mascareñas, *Nat. Commun.* **2016**, *7*, 12538, https://doi.org/10.1038/ncomms12538.
[66] A. J. Kowaltowski, F. Abdulkader, *Biophys. J.* **2024**, *123*, 4150–4157, https://doi.org/10.1016/j.bpj.2024.03.011.
[67] N. Ng, M. C. Cabral-da-Silva, S. Maksour, T. Berg, M. Engel, D. M. Silva, D. Do-Ha, J. S. Lum, S. S. Muñoz, N. Suarez-Bosche, C. H. Stevens, L. Ooi, *Transl. Med. Commun.* **2020**, *5*, 18, https://doi.org/10.1186/s41231-020-00071-0.
[68] Z. Liu, H. Zou, Q. Dang, H. Xu, L. Liu, Y. Zhang, J. Lv, H. Li, Z. Zhou, X. Han, *Mol. Cancer* **2022**, *21*, 220, https://doi.org/10.1186/s12943-022-01680-z.
[69] Y. Xu, Y. Wang, F. S. Liang, *Angew. Chem. Int. Ed.* **2023**, *62*, e202309291.
[70] M. M. Pomaville, C. He, *Trends Cancer* **2023**, *9*, 528–542, https://doi.org/10.1016/j.trecan.2023.04.003.
[71] L. Lan, Y. J. Sun, X. Y. Jin, L. J. Xie, L. Liu, L. Cheng, *Angew. Chem. Int. Ed.* **2021**, *60*, 18116–18121, https://doi.org/10.1002/anie.202103854.
[72] T. Wang, T. Hong, Y. Huang, H. Su, F. Wu, Y. Chen, L. Wei, W. Huang, X. Hua, Y. Xia, J. Xu, J. Gan, B. Yuan, Y. Feng, X. Zhang, C.-G. Yang, X. Zhou, *J. Am. Chem. Soc.* **2015**, *137*, 13736–13739, https://doi.org/10.1021/jacs.5b06690.
[73] W. Hao, M. Dian, Y. Zhou, Q. Zhong, W. Pang, Z. Li, Y. Zhao, J. Ma, X. Lin, R. Luo, Y. Li, J. Jia, H. Shen, S. Huang, G. Dai, J. Wang, Y. Sun, D. Xiao, *Nat. Commun.* **2022**, *13*, 5845, https://doi.org/10.1038/s41467-022-32963-0.
[74] X. Deng, Y. Qing, D. Horne, H. Huang, J. Chen, *Nat. Rev. Clin. Oncol.* **2023**, *20*, 507–526, https://doi.org/10.1038/s41571-023-00774-x.
[75] S. Jin, X. Zhang, Y. Miao, P. Liang, K. Zhu, Y. She, Y. Wu, D. A. Liu, J. Huang, J. Ren, J. Cui, *Cell Res.* **2018**, *28*, 955–957, https://doi.org/10.1038/s41422-018-0069-8.

Manuscript received: July 11, 2025
Revised manuscript received: October 24, 2025
Manuscript accepted: October 27, 2025
Version of record online: November 05, 2025

© 2025 Wiley-VCH GmbH

15213773, 2025, 51, Downloaded from https://onlinelibrary.wiley.com/doi/10.1002/anie.202515137 by Shanghai Institute Of Organic Chemistry, Wiley Online Library on [16/12/2025]. See the Terms and Conditions (https://onlinelibrary.wiley.com/terms-and-conditions) on Wiley Online Library for rules of use; OA articles are governed by the applicable Creative Commons License